Methodology for Smooth Connection of Doubly Fed Induction Generators to the Grid

Gerardo Tapia, Giovanna Santamaría, Mikel Telleria, and Ana Susperregui, *Member, IEEE*

***Abstract*—A systematic methodology for smooth connection of wind-turbine-driven doubly fed induction generators (DFIGs) to the grid is presented. Synchronization of the voltage induced in the DFIG open stator to that of the grid, which needs to be accomplished prior to connection, is thoroughly examined. A particular grid-voltage-oriented rotor control scheme is considered for this purpose. Generic tuning equations for the rotor current integral–proportional (I-P) controllers involved in this scheme are also derived. Transition between the control configurations devoted to synchronization and normal operation—active power generation and reactive power interchange with the grid—at the instant of connection is studied in detail. Mainly due to the reference frame selected for synchronization, the greater part of this transition takes place naturally. However, given that the rotor current dynamics vary significantly depending on whether the DFIG stator is connected to the grid or not, the parameters of the I-P controllers involved in both schemes will accordingly be different. Consequently, a "bumpless" strategy is provided that preserves the smoothness of the connection. A simple method for initial rotor positioning, required when performing vector control based on an incremental encoder, is also suggested. The resulting overall methodology is validated on a 7-kW DFIG-based laboratory-scale test bench.**

***Index Terms*—Doubly fed induction generators (DFIGs), industrial power system control, initial rotor positioning, smooth connection, synchronization, vector control, wind power generation.**

NOMENCLATURE

–	Subscript.
$\vec{i}_{ms}$	Stator magnetizing current space phasor.
$i_{r\_}$, $i_{s\_}$	Rotor and stator direct- or quadrature-axis current components, expressed in a particular reference frame.
$\vec{i}_{r\_}$, $\vec{i}_{s\_}$	Rotor and stator current space phasors, expressed in a particular reference frame.
L_m, L_r, L_s	Magnetizing, rotor, and stator inductances.
L'_r	Rotor transient inductance.
P_s, Q_s	Stator-side active and reactive powers.
R_r, R_s	Rotor and stator resistances.
$v_{r\_}$, $v_{s\_}$	Rotor and stator direct- or quadrature-axis voltage components, expressed in a particular reference frame.
$\vec{v}_{r\_}$, $\vec{v}_{s\_}$	Rotor and stator voltage space phasors, expressed in a particular reference frame.
ρ_s	Angle between the stator-flux-oriented and the stationary reference frames.
ρ'_s	Angle between the grid-voltage-oriented and the stationary reference frames.
σ	Total leakage factor.
ω_g	Angular speed of the generic reference frame.
ω_{ms}	Angular speed of the stator flux space phasor.
ω_s	Synchronous angular frequency of the grid.
ω_r	Rotor electrical speed.
ω_{sl}	Angular slip frequency.
$\vec{\psi}_{r\_}$, $\vec{\psi}_{s\_}$	Rotor and stator flux space phasors, expressed in a particular reference frame.

Subscripts

D, Q	Direct- and quadrature-axis components, expressed in the stationary reference frame.
g	Space phasor expressed in a generic reference frame.
v_{grid}	Space phasor expressed in a grid-voltage-oriented reference frame.
x, y	Direct- and quadrature-axis components, expressed in the stator-flux-oriented reference frame.
x', y'	Direct- and quadrature-axis components, expressed in a grid-voltage-oriented reference frame.
α, β	Direct- and quadrature-axis components, expressed in the rotor natural reference frame.
ψ_s	Space phasor expressed in the stator-flux-oriented reference frame.

Manuscript received January 13, 2009; revised April 1, 2009. First published October 23, 2009; current version published November 20, 2009. Paper no. TEC-00517-2008.

G. Tapia and A. Susperregui are with the Department of Systems Engineering and Control, Polytechnical University College, University of the Basque Country, 20018 Donostia-San Sebastián, Spain (e-mail: gerardo.tapia@ehu.es; ana.susperregui@ehu.es).

G. Santamaría is with Jesús María Aguirre, SA (JEMA), 20160 Lasarte-Oria, Spain (e-mail: g.santamaria@grupojema.com).

M. Telleria was with Jesus Maria Aguirre, SA (JEMA), 20160 Lasarte-Oria, Spain. He is now with GAMESA, 31621 Sarriguren, Spain (e-mail: mtelleria@gamesacorp.com).

Digital Object Identifier 10.1109/TEC.2009.2025334

I. INTRODUCTION

THE DOUBLY fed induction machine is widely used in variable-speed wind generation systems. Due to a back-to-back double-bridge converter configuration feeding its wound

0885-8969/$26.00 © 2009 IEEE

rotor, it is made possible to manage the slip power. In this way, its stator is kept directly connected to the grid within a certain operation range, covering from subsynchronous to supersynchronous rotating speeds. Given that only the slip power has to be handled by the bidirectional rotor converter, it is sufficient to size it so that it typically supports between 25% and 30% of the doubly fed induction generator (DFIG) rated power [1]–[4].

In addition, when commanded by appropriate vector control algorithms, this converter configuration allows governing separately the generated active power and the reactive power exchanged between the DFIG and the grid it is connected to. In this context, the reference value of the active power to be generated is generally fixed aiming at optimizing energy extraction at any wind speed. On the other hand, considering their ability to operate even with capacitive power factors, DFIGs can be regarded as continuous sources of reactive power. Consequently, wind farms made up of DFIGs can contribute to keep the voltage of the grid within acceptable limits through the application of secondary voltage regulation strategies [5].

Given that the double-bridge rotor converter is conceived to manage a slip power up to 25% or 30% of the wind generator rated power, a DFIG is kept connected to the grid as long as its rotational speed remains within a certain range. Hence, a DFIG is connected to the grid when the wind is strong enough to extract energy from it profitably. On the other hand, if the wind power exceeds the rated power of the wind generator in a way that pitch regulation becomes inefficient to account for excess power, it is unavoidable to disconnect the DFIG from the grid. The outlined scenario leads to quite often connections (and disconnections) of DFIGs to (from) the grid, even in sites where wind conditions are not extremely variable.

Even though wind-turbine-driven DFIGs are, in fact, asynchronous machines, the bidirectional rotor converter managing the slip power makes them behave as if they were actually synchronous generators. As a consequence, prior to connecting the stator of a DFIG to the grid, it is necessary to synchronize the voltage induced at its stator terminals to that of the grid.

Diverse control strategies for wind-turbine-driven DFIGs have been proposed by different authors over the last decade, some of which constitute real alternatives to classical vector control schemes based on encoder and proportional–integral (PI) regulators [4]. Among others, various robust control techniques have been explored, some of which correspond to output feedback [6], [7], different approaches to variable structure control (VSC) [8]–[10], and discrete pole placement with the sensitivity function shaping method, which is known also as RST control [11]. At the same time, other control and estimation schemes, which are commonly applied to electric drives like "sensorless" [12]–[16] and direct torque control (DTC) [17], [18], have also been adopted in the particular case of DFIGs.

However, the majority of the control configurations put forward in the literature address solely the operation mode in which the stator of the DFIG is already connected to the grid, and therefore exchange power. Only a few contributions have outlined or described in some detail possible strategies for smooth connection of DFIGs to the grid. So far, the synchronization problem has been tackled from different viewpoints, hence giving rise to alternative methods as open-loop stator voltage control [13], closed-loop regulation of rotor current [6], [7], [19], and phase-locked loop (PLL) [20]–[23] or even DTC [18] command of the voltage induced at the open stator.

This paper proposes a systematic approach for smooth connection of DFIGs to the grid. In particular, the control configuration devised for synchronizing the voltage induced in the DFIG open stator to that of the grid is justified and analyzed in depth. A method to tune the controllers present in this configuration is also provided. Special attention is paid to practical issues such as initial rotor positioning and "bumpless" transition between control schemes at the instant of connection. Experimental results, which are obtained by the implementation of the suggested connection methodology on a 7-kW laboratory-scale DFIG, are presented to support the appropriateness of the proposed approach.

II. DFIG Model in the Stator-Flux-Oriented Reference Frame

The voltage equations of a DFIG, expressed in phasor form according to a generic reference frame rotating at ω_g angular speed, are given by [24], [25]

$$\vec{v}_{sg} = R_s \vec{\imath}_{sg} + \frac{d\vec{\psi}_{sg}}{dt} + j\omega_g \vec{\psi}_{sg} \tag{1}$$

$$\vec{v}_{rg} = R_r \vec{\imath}_{rg} + \frac{d\vec{\psi}_{rg}}{dt} + j\left(\omega_g - \omega_r\right)\vec{\psi}_{rg} \tag{2}$$

where

$$\vec{\psi}_{sg} = L_s \vec{\imath}_{sg} + L_m \vec{\imath}_{rg} \tag{3}$$

$$\vec{\psi}_{rg} = L_r \vec{\imath}_{rg} + L_m \vec{\imath}_{sg}. \tag{4}$$

Aiming at facilitating both the design and implementation of a decoupled active and reactive power control system for the DFIG, the expressions before are particularized to the stator-flux-oriented reference frame, thus yielding

$$\vec{v}_{s\psi_s} = R_s \vec{\imath}_{s\psi_s} + \frac{d\vec{\psi}_{s\psi_s}}{dt} + j\omega_{ms}\vec{\psi}_{s\psi_s} \tag{5}$$

$$\vec{v}_{r\psi_s} = R_r \vec{\imath}_{r\psi_s} + \frac{d\vec{\psi}_{r\psi_s}}{dt} + j\left(\omega_{ms} - \omega_r\right)\vec{\psi}_{r\psi_s} \tag{6}$$

with

$$\vec{\psi}_{s\psi_s} = L_s \vec{\imath}_{s\psi_s} + L_m \vec{\imath}_{r\psi_s} = L_m \vec{\imath}_{ms} \tag{7}$$

$$\vec{\psi}_{r\psi_s} = L_r \vec{\imath}_{r\psi_s} + L_m \vec{\imath}_{s\psi_s}. \tag{8}$$

Given that the stator-side active and reactive powers of the DFIG are controlled by commanding the current fed into its rotor, the stator current in (5), (6), and (8) is expressed, by virtue of (7), as a function of the stator magnetizing and rotor currents as

$$\vec{\imath}_{s\psi_s} = \frac{L_m\left(\vec{\imath}_{ms} - \vec{\imath}_{r\psi_s}\right)}{L_s}. \tag{9}$$

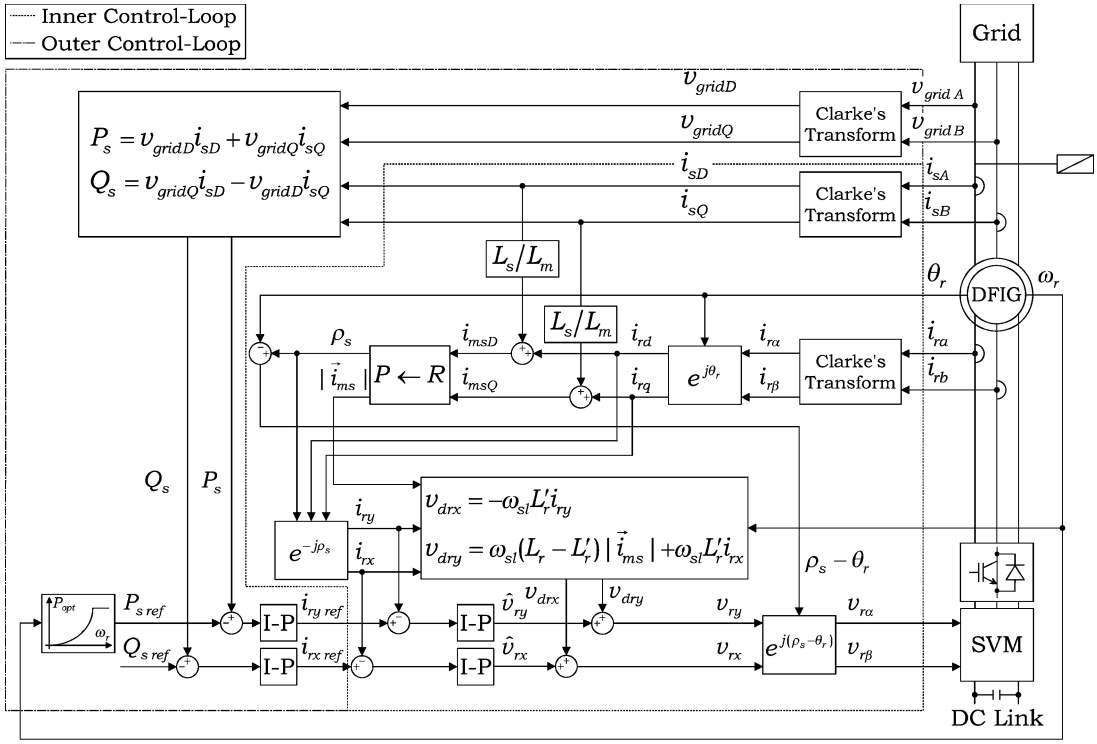

Fig. 1. Control scheme for normal operation.

Accordingly, voltage equations (5) and (6) are rewritten as follows:

$$\vec{v}_{s\psi_s} = \frac{R_s L_m}{L_s}\left(\vec{i}_{ms} - \vec{i}_{r\psi_s}\right) + L_m \frac{d\vec{i}_{ms}}{dt} + j\omega_{ms} L_m \vec{i}_{ms} \tag{10}$$

$$\vec{v}_{r\psi_s} = R_r \vec{i}_{r\psi_s} + L'_r \frac{d\vec{i}_{r\psi_s}}{dt} + \frac{L_m^2}{L_s}\frac{d\vec{i}_{ms}}{dt} + j\omega_{sl} L'_r \vec{i}_{r\psi_s} + j\omega_{sl}\frac{L_m^2}{L_s}\vec{i}_{ms} \tag{11}$$

where $L'_r = \sigma L_r$, $\sigma = 1 - L_m^2/(L_s L_r)$, and $\omega_{sl} = \omega_{ms} - \omega_r$.

Considering that, by definition, the direct axis of the stator-flux-oriented reference frame is collinear with both $\vec{\psi}_s$ and $\vec{i}_{ms}$, decomposing vector expressions (10) and (11) into their direct- (x) and quadrature-axis (y) components produces

$$v_{sx} = \frac{R_s L_m}{L_s}\left(|\vec{i}_{ms}| - i_{rx}\right) + L_m \frac{d\,|\vec{i}_{ms}|}{dt} \tag{12}$$

$$v_{sy} = -\frac{R_s L_m}{L_s} i_{ry} + \omega_{ms} L_m\, |\vec{i}_{ms}| \tag{13}$$

$$v_{rx} = R_r i_{rx} + L'_r \frac{di_{rx}}{dt} + \left(L_r - L'_r\right)\frac{d\,|\vec{i}_{ms}|}{dt} - \omega_{sl} L'_r i_{ry} \tag{14}$$

$$v_{ry} = R_r i_{ry} + L'_r \frac{di_{ry}}{dt} + \omega_{sl}\left(L_r - L'_r\right)|\vec{i}_{ms}| + \omega_{sl} L'_r i_{rx}. \tag{15}$$

Equations (14) and (15), which reflect the dynamics of the DFIG i_{rx} and i_{ry} current components, constitute the basis for the design and implementation of the stator-side decoupled active and reactive power control structure sketched in Fig. 1, where SVM indicates space-vector modulation [26], [27]. The realization of this control configuration is detailed in [28], and a procedure to tune its integral–proportional (I-P) controllers analytically is provided in [29].

In order to grasp the synchronization method described in the next section, it is, however, fundamental to draw attention to a particular feature of the DFIG behavior when its stator current equals zero. This situation corresponds to two possible operational modes.

1) The stator of the DFIG is open, and disconnected from the grid.
2) Although the stator of the DFIG is connected to the grid, they do not exchange any power.

Consequently, assuming that $\vec{i}_{s\psi_s} = 0$ in (7), it turns out that

$$\vec{\psi}_{s\psi_s} = L_m \vec{i}_{r\psi_s} = L_m \vec{i}_{ms} \tag{16}$$

which evidences that, as expected, the stator magnetizing and rotor currents coincide, and that the rotor current space phasor is aligned with the stator flux space phasor. As a result,

$$i_{rx} = |\vec{i}_{ms}| \qquad i_{ry} = 0. \tag{17}$$

Moreover, substitution of (17) in both (12) and (13) leads to

$$v_{sx} = L_m \frac{di_{rx}}{dt} \tag{18}$$

$$v_{sy} = \omega_{ms} L_m i_{rx} \tag{19}$$

thus revealing that, once in steady state—i.e., $di_{rx}/dt = 0$—v_{sx} vanishes to zero, and stator voltage space phasor $\vec{v}_s$ turns out to be in quadrature with rotor current space phasor $\vec{i}_r$.

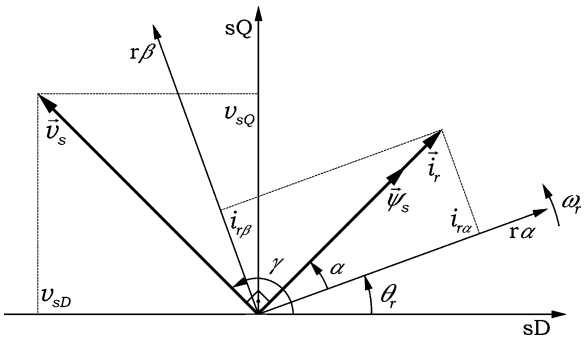

Fig. 2. Steady-state relative positions of $\vec{v}_s$, $\vec{i}_r$, and $\vec{\psi}_s$ for zero stator current.

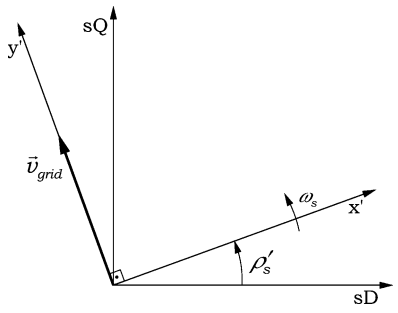

Fig. 3. Grid-voltage-oriented reference frame.

In summary, when the stator current equals zero, the steady-state relative positions of stator voltage, rotor current, and stator flux space phasors are those displayed in Fig. 2.

III. Synchronization

It is obvious that, in order to ensure smooth connection of the DFIG to the grid, the three-phase voltage induced in its stator must coincide with the grid voltage in amplitude, frequency, and phase. For this purpose, an appropriate three-phase current must be fed into the DFIG rotor. In addition, at the instant of connecting the DFIG stator to the grid, zero-power exchange must be guaranteed.

A. DFIG Model for Synchronization

With the aim of synchronizing the voltage induced in the DFIG stator with that of the grid, it is evidently required to keep track of the grid voltage space phasor $\vec{v}_{\rm grid}$ all the time. Therefore, it seems judicious to consider that a grid-voltage-oriented reference frame should be specified to carry out the synchronization process. In particular, the synchronously rotating reference frame x'–y' displayed in Fig. 3, whose quadrature y' axis is collinear with the grid voltage space phasor, is considered here.

Given that during synchronization the DFIG stator remains open, and consequently, the stator current equals zero, particularization of (1)–(4) to the aforementioned grid-voltage-oriented reference frame leads to the following vector equations:

$$\vec{v}_{sv_{\rm grid}} = \frac{d\vec{\psi}_{sv_{\rm grid}}}{dt} + j\omega_s\vec{\psi}_{sv_{\rm grid}} \tag{20}$$

$$\vec{v}_{rv_{\rm grid}} = R_r\vec{i}_{rv_{\rm grid}} + \frac{d\vec{\psi}_{rv_{\rm grid}}}{dt} + j\left(\omega_s-\omega_r\right)\vec{\psi}_{rv_{\rm grid}} \tag{21}$$

where

$$\vec{\psi}_{sv_{\rm grid}} = L_m\vec{i}_{rv_{\rm grid}} \tag{22}$$

$$\vec{\psi}_{rv_{\rm grid}} = L_r\vec{i}_{rv_{\rm grid}}. \tag{23}$$

Substitution of (22) and (23) into (20) and (21) produces the voltage equations given as follows:

$$\vec{v}_{sv_{\rm grid}} = L_m\frac{d\vec{i}_{rv_{\rm grid}}}{dt} + j\omega_s L_m\vec{i}_{rv_{\rm grid}} \tag{24}$$

$$\vec{v}_{rv_{\rm grid}} = R_r\vec{i}_{rv_{\rm grid}} + L_r\frac{d\vec{i}_{rv_{\rm grid}}}{dt} + j\left(\omega_s-\omega_r\right)L_r\vec{i}_{rv_{\rm grid}} \tag{25}$$

which decomposed into their direct- (x') and quadrature-axis (y') components result in

$$v_{sx'} = L_m\frac{di_{rx'}}{dt} - \omega_s L_m i_{ry'} \tag{26}$$

$$v_{sy'} = L_m\frac{di_{ry'}}{dt} + \omega_s L_m i_{rx'} \tag{27}$$

$$v_{rx'} = R_r i_{rx'} + L_r\frac{di_{rx'}}{dt} - \left(\omega_s-\omega_r\right)L_r i_{ry'} \tag{28}$$

$$v_{ry'} = R_r i_{ry'} + L_r\frac{di_{ry'}}{dt} + \left(\omega_s-\omega_r\right)L_r i_{rx'}. \tag{29}$$

In space-phasor terms, synchronization demands that the $\vec{v}_s$ space vector corresponding to the voltage induced at the terminals of the open stator matches that of the grid voltage $\vec{v}_{\rm grid}$, i.e., $\vec{v}_s = \vec{v}_{\rm grid}$. Since $\vec{v}_{\rm grid}$ is, by definition, aligned with the y' axis, the latter requirement could be formulated as

$$v_{sx'} = 0 \qquad v_{sy'} = \left|\vec{v}_{\rm grid}\right|. \tag{30}$$

Examination of (26) and (27) reveals that, once in steady state, the two conditions in (30) are satisfied provided that

$$i_{rx'} = \frac{\left|\vec{v}_{\rm grid}\right|}{\omega_s L_m} \qquad i_{ry'} = 0. \tag{31}$$

As a consequence, the synchronization task might be viewed as a problem of regulating rotor current $i_{rx'}$ and $i_{ry'}$ components at their respective set points of $i_{rx'\,\rm ref} = \left|\vec{v}_{\rm grid}\right| / \left(\omega_s L_m\right)$ and $i_{ry'\,\rm ref} = 0$.

It is essential to note that, after synchronization is achieved, the stator-flux-oriented reference frame coincides exactly with the grid-voltage-oriented reference frame, i.e., $x = x'$ and $y = y'$. In effect, according to (31), the rotor current space phasor is aligned with x'. But, as displayed in Fig. 2, in open stator, the rotor current space phasor is collinear with that of the stator flux—which is, by definition, aligned with x. Therefore, once synchronization is reached, all x', $\vec{i}_r$, $\vec{\psi}_s$, and x turn out to be collinear, and

$$i_{rx} \equiv i_{rx'} = \frac{\left|\vec{v}_{\rm grid}\right|}{\omega_s L_m} \qquad i_{ry} \equiv i_{ry'} = 0. \tag{32}$$

Furthermore, it is well known that, when the DFIG stator is connected to the grid, the active and reactive powers exchanged

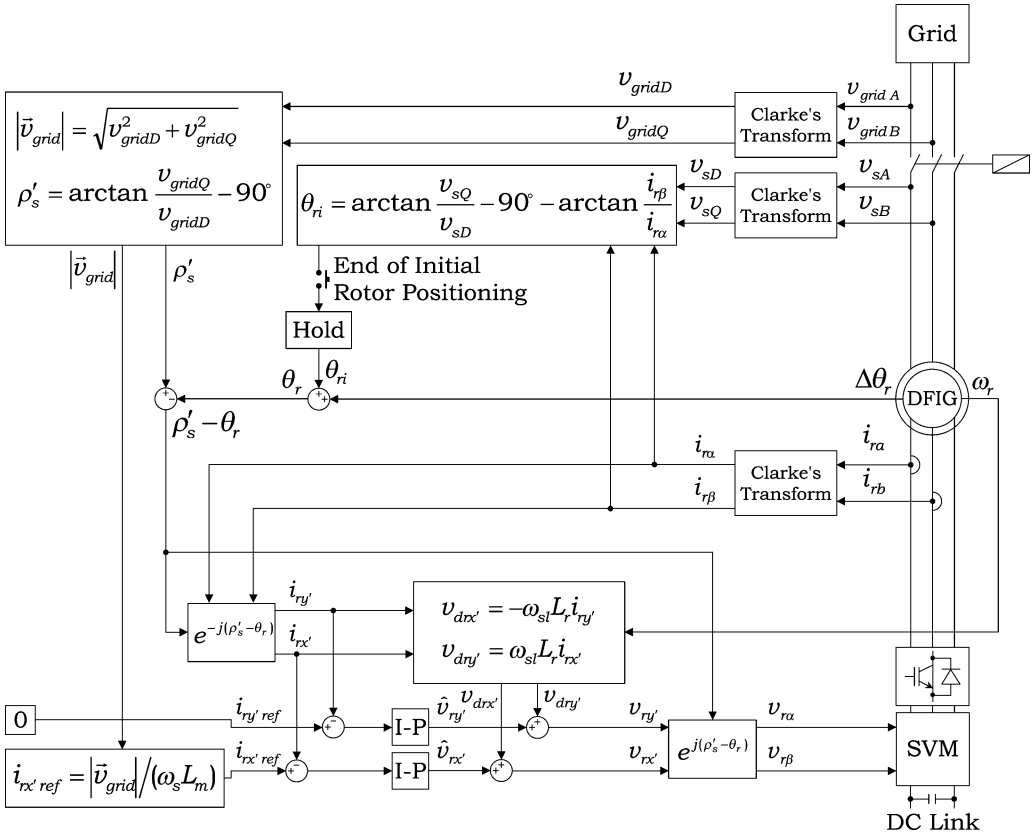

Fig. 4. Control scheme for initial rotor positioning and synchronization.

between them may be computed as [24], [25]

$$P_s = -\frac{3}{2}\left|\vec{v}_{\rm grid}\right| i_{ry} \tag{33}$$

$$Q_s = \frac{3}{2}\left|\vec{v}_{\rm grid}\right|\left(\left|\vec{i}_{ms}\right| - i_{rx}\right) \tag{34}$$

where the modulus of the stator magnetizing current space phasor is given by $\left|\vec{i}_{ms}\right| = \left|\vec{v}_{\rm grid}\right| / \left(\omega_s L_m\right)$. Therefore, note that the values provided for i_{rx} and i_{ry} in (32) lead to zero-power exchange between the DFIG stator and the grid. This implies that, when, after achieving synchronization, the DFIG stator is connected to the grid at zero power—with set points $P_{s\,\rm ref} = Q_{s\,\rm ref} = 0$ in Fig. 1—the active and reactive power I-P controllers will naturally produce set points $i_{rx\,\rm ref} = \left|\vec{i}_{ms}\right|$ and $i_{ry\,\rm ref} = 0$, which coincide with the values already reached by i_{rx} and i_{ry} during synchronization.

The latter consideration, added to that concerning the alignment of x' and x, leads to the conclusion that a smooth transition between the control systems devoted to synchronization and normal operation of the DFIG is guaranteed at the moment of connecting its stator to the grid.

B. Control Scheme for Synchronization

Fig. 4 shows the control system proposed for synchronization. As suggested in the previous section, it basically consists in a rotor current regulator that seeks to satisfy (31). In fact, it is very similar to the inner control loop displayed in Fig. 1. The key difference arises due to the fact that the rotor current is now regulated in a new reference frame x'–y', and consequently, the way of deriving ρ'_s differs substantially from that in which ρ_s is estimated.

It is also fundamental to note that the dynamics of the DFIG rotor current are rather different depending on whether its stator is connected to the grid or not. Examination of (14) and (15) in comparison to (28) and (29) shows that, although the dynamics are first order in both cases, the resulting time constants, as well as the voltage coupling terms, are different. Accordingly, even if the structure of the rotor current control system is kept, the gains of its I-P's and the decoupling voltage terms are modified depending on whether the DFIG is in synchronization or normal operation.

In particular, during synchronization, the following voltage components are applied to the DFIG rotor:

$$v_{rx'} = \hat{v}_{rx'} + v_{drx'} \tag{35}$$

$$v_{ry'} = \hat{v}_{ry'} + v_{dry'} \tag{36}$$

where, as shown in Fig. 4, $\hat{v}_{rx'}$ and $\hat{v}_{ry'}$ are generated through the two I-P's in charge of regulating the rotor current, and decoupling voltages $v_{drx'}$ and $v_{dry'}$ are computed as

$$v_{drx'} = -\left(\omega_s - \omega_r\right) L_r i_{ry'} \tag{37}$$

$$v_{dry'} = \left(\omega_s - \omega_r\right) L_r i_{rx'}. \tag{38}$$

Considering the two latter expressions, substitution of (35) and (36) into (28) and (29), respectively, leads to

$$\hat{v}_{rx'} = R_r i_{rx'} + L_r \frac{di_{rx'}}{dt} \tag{39}$$

$$\hat{v}_{ry'} = R_r i_{ry'} + L_r \frac{di_{ry'}}{dt}. \tag{40}$$

Hence, the first-order transfer function given next is established between the rotor current components and those of the voltage generated by the I-P controllers

$$\frac{I_{rx'}(s)}{\hat{V}_{rx'}(s)} = \frac{I_{ry'}(s)}{\hat{V}_{ry'}(s)} = \frac{1/R_r}{1 + (L_r/R_r)s} \tag{41}$$

which proves that the dynamics are the same in both x' and y' axes. Accordingly, two identical controllers are employed to regulate $i_{rx'}$ and $i_{ry'}$. More specifically, the following I-P structure is adopted:

$$\hat{V}_{rx'}(s) = -K_p I_{rx'}(s) + \frac{K_p}{T_i} \frac{I_{rx'\,\mathrm{ref}}(s) - I_{rx'}(s)}{s} \tag{42}$$

which is also valid for the y' axis, provided that subscript x' is replaced by y'.

Thus, appropriate combination of (41) and (42) leads to the following identical closed-loop transfer functions for current components $i_{rx'}$ and $i_{ry'}$:

$$\frac{I_{rx'}(s)}{I_{rx'\,\mathrm{ref}}(s)} = \frac{I_{ry'}(s)}{I_{ry'\,\mathrm{ref}}(s)} = \frac{K_p/(T_i L_r)}{s^2 + ((K_p + R_r)/L_r)s + K_p/(T_i L_r)} \tag{43}$$

whose static gain is equal to 1. This feature guarantees the absence of steady-state errors in $i_{rx'}$ and $i_{ry'}$.

The I-P controller parameters are then tuned through pole placement, so as to achieve the desired closed-loop transfer function given by

$$\frac{I_{rx'}(s)}{I_{rx'\,\mathrm{ref}}(s)} = \frac{I_{ry'}(s)}{I_{ry'\,\mathrm{ref}}(s)} = \frac{\omega_{nd}^2}{s^2 + 2\xi_d \omega_{nd} s + \omega_{nd}^2} \tag{44}$$

which exhibits ξ_d damping factor and ω_{nd} natural frequency. Consequently, equating the characteristic polynomial coefficients of transfer functions (43) and (44) individually, the following tuning equations arise:

$$K_p = 2\xi_d \omega_{nd} L_r - R_r \tag{45}$$

$$T_i = \frac{K_p}{L_r \omega_{nd}^2}. \tag{46}$$

In particular, a $\xi_d = 1$ damping factor is selected in this paper, hence avoiding the presence of overshoots during transients. Regarding ω_{nd}, it is established through the definition of a target t_{sd} settling time for $i_{rx'}$ and $i_{ry'}$ control loops. In fact, according to the 2% criterion [30], $\omega_{nd} = 5.8/t_{sd}$ results for critically damped systems.

Tuning equations (45) and (46) are extremely similar to those used to adjust the control loops of i_{rx} and i_{ry} for normal operation—see [29]. The only difference is caused by the time constant of the rotor circuit, which equals $T_r = L_r/R_r$ when the DFIG stator is disconnected from the grid—see (41)—and turns into $T_r' = L_r'/R_r$ when it is connected—see (14) and (15). Since $L_r' < L_r$, the open-loop dynamics of the rotor circuit turn out to be faster when the DFIG is in normal operation, with its stator connected to the grid. In accordance, a shorter closed-loop settling time will, in general, be demandable to rotor current during normal operation. In other words, it is reasonable to admit that the value of the target t_{sd} settling time chosen for synchronization should be more conservative than that selected for normal operation. This obviously results in different values being assigned to parameters K_p and T_i depending on whether the DFIG is in synchronization or in normal operation. It is, therefore, essential to consider that, in order to avoid spoiling smooth connection of the DFIG stator to the grid, a "bumpless" transition between both controllers must also be provided.

Once the resulting I-P current controller in (42) is discretized following the Tustin's trapezoidal method [31], it is realized based on difference equations expressed according to the direct noncanonical form given as follows [32]:

$$\begin{aligned}\hat{v}_{rx'}(k) = \hat{v}_{rx'}(k-1) + K_{pi}\left[i_{rx'\,\mathrm{ref}}(k) + i_{rx'\,\mathrm{ref}}(k-1)\right] \\ - \left(K_p + K_{pi}\right) i_{rx'}(k) + \left(K_p - K_{pi}\right) i_{rx'}(k-1)\end{aligned} \tag{47}$$

where index k stands for kth sampling instant, $K_{pi} = K_p T_s/(2T_i)$, and T_s is the sample time. Equation (47) is also applicable to the y' axis after replacing subscript x' with y'.

IV. Initial Rotor Positioning

As reflected in Figs. 1 and 4, the global control system of the DFIG requires the knowledge of rotor electrical position θ_r for both synchronization and normal operation. Note that an incremental encoder provides just a measure of the relative angle rotated with respect to a certain initial angular position of the rotor θ_{ri}. As a result, the value of the electrical angle obtained by means of an encoder will only equal θ_r if the rotor and the stationary reference frames are initially aligned—$\theta_{ri} = 0$. But this is not obviously the most common situation; it is rather a coincidence.

Therefore, prior to launching the synchronization process, it is required to identify the initial rotor position θ_{ri} at some instant. From this moment onward, the encoder will measure the increment of the electrical angle $\Delta\theta_r(t)$ with respect to θ_{ri}, and $\theta_r(t)$ will be derived just by adding θ_{ri} to $\Delta\theta_r(t)$.

When the DFIG stator is disconnected from the grid, it is not difficult to provide a reliable estimate of θ_r at a certain instant. It is sufficient to feed the DFIG rotor with a three-phase balanced voltage and to measure the resulting steady-state rotor current, as well as the voltage induced at the terminals of the open stator. In fact, according to Fig. 2, the initial rotor position from which the encoder starts measuring the electrical angle increment may be estimated as

$$\theta_{ri} = \gamma - 90^{\mathrm{o}} - \alpha \tag{48}$$

where $\gamma = \arctan(vsQ/vsD)$ and $\alpha = \arctan(i_{r\beta}/i_{r\alpha})$.

This preliminary stage of initial rotor positioning is not necessary if DFIG "sensorless" control schemes like those proposed in [12]–[16] and [24] are adopted. In this case, given that the

estimated θ_r converges spontaneously to its actual value, it is just required to allow enough time for the rotor position observer to converge before initiating the synchronization process.

V. Task Sequence for Smooth Connection

From the considerations in the previous sections, it follows that smooth connection of the DFIG stator to the grid can be guaranteed provided that the sequence of tasks given next is accomplished.

1) Typically, when the generator rotational speed exceeds a certain threshold value, it is assumed that the wind is strong enough to generate electric power profitably, and the global control system produces an order of connecting the DFIG stator to the grid.
2) The initial rotor positioning is then carried out, which provides an estimate of the rotor electrical position at a certain instant θ_{ri}. From this very instant onward, the incremental encoder measures the $\Delta\theta_r(t)$ angle rotated with respect to θ_{ri}, and $\theta_r(t)$ is derived by summation of both angles.
   In "sensorless" schemes, the algorithm for estimating θ_r is started, and sufficient time is allowed for the estimator to converge.
3) Synchronization is performed by applying the rotor current command strategy detailed in Section III. Recall that, once synchronization is reached, the grid-voltage- and stator-flux-oriented reference frames coincide. In addition, $i_{rx} \equiv i_{rx'} = |\vec{i}_{ms}|$ and $i_{ry} \equiv i_{ry'} = 0$.
4) The DFIG stator is connected to the grid at zero power by setting $P_{s\,\mathrm{ref}} = Q_{s\,\mathrm{ref}} = 0$ in the control configuration in Fig. 1. At the instant of connection, the control scheme is switched from that in Fig. 4 to that displayed in Fig. 1. Yet, this transition takes places smoothly since, prior to connection, the following hold.
   a) $i_{rx} \equiv i_{rx'}$ and $i_{ry} \equiv i_{ry'}$.
   b) The steady-state values of i_{ry} and i_{rx} already match the set points $i_{ry\,\mathrm{ref}} = 0$ and $i_{rx\,\mathrm{ref}} = |\vec{i}_{ms}|$ that will later be fixed by the active and reactive power I-P controllers when connecting the DFIG stator to the grid at zero power.

   However, decoupling voltages, as well as parameters K_p and T_i of rotor current controllers, do, in general, vary when switching from the control scheme depicted in Fig. 4 to that in Fig. 1. Despite the previously mentioned cautions, this sole change may cause large "bumps" of rotor voltage at the instant of connecting the DFIG stator to the grid. This would obviously result in a highly deficient connection.
   This unwanted phenomenon can be removed just by carrying out a "bumpless" transition between both control systems. For this purpose, assuming that switching from one scheme to the other occurs at the kth sampling instant, it is sufficient to ensure that

$$v_{rx}(k) = v_{rx'}(k-1) \qquad v_{ry}(k) = v_{ry'}(k-1). \tag{49}$$

TABLE I
DFIG Electric Parameters

Parameter	Value
Rated r.m.s. stator voltage	220/380 V
Rated peak stator current	27.7/16 A
Rated peak rotor voltage	190 V
Rated peak rotor current	24.5 A
Stator resistance per phase, R_s	375 mΩ
Stator inductance per phase, L_s	83.808 mH
Magnetizing inductance, L_m	40.318 mH
Rotor resistance per phase, R_r	175 mΩ
Rotor inductance per phase, L_r	20.931 mH
General turns ratio, n	2.001
Number of pole pairs, P	2

From the requirements mentioned before, it follows that the outputs of the rotor current I-P controllers at the kth sampling instant should be forced to be

$$\hat{v}_{rx}(k) = v_{rx'}(k-1) - v_{drx}(k) \tag{50}$$

$$\hat{v}_{ry}(k) = v_{ry'}(k-1) - v_{dry}(k) \tag{51}$$

where decoupling voltages v_{drx} and v_{dry}, which are easily identifiable in (14) and (15), are computed as follows [29]:

$$v_{drx} = -\omega_{sl} L'_r i_{ry} \tag{52}$$

$$v_{dry} = \omega_{sl}(L_r - L'_r)|\vec{i}_{ms}| + \omega_{sl} L'_r i_{rx} \tag{53}$$

as reflected in Fig. 1.

5) The DFIG is now ready to exchange active and reactive powers with the grid through its stator.

Note that disconnecting the DFIG stator from the grid does not involve any additional problem, since it is only required to guarantee zero-power exchange at the disconnection instant.

VI. Experimental Results

The experimental rig built to test the performance of the proposed overall control strategy is first described in this section. Subsequently, some of the most representative and meaningful results related to its performance are presented and evaluated in depth.

A. Description of the Experimental Setup

The core of the laboratory-scale test bench is a 7-kW DFIG whose rotor shaft is coupled to that of a 15-kW armature-controlled dc motor. The rotating speed of the dc motor, whose purpose is to drive the DFIG, is governed at will by means of a commercially available controller. A conventional lamp synchronoscope is also provided, which visually informs about the course of the synchronization stage. The main electric parameters of the DFIG are those collected in Table I.

The algorithms for initial rotor positioning and synchronization, which are covered in detail in Sections IV and III, as well as that aiming at controlling active and reactive powers separately, as presented in [28] and [29], are all programmed in DSP TMS320VC5402 by Texas Instruments Incorporated. The greater part of the resulting program is written in C language,

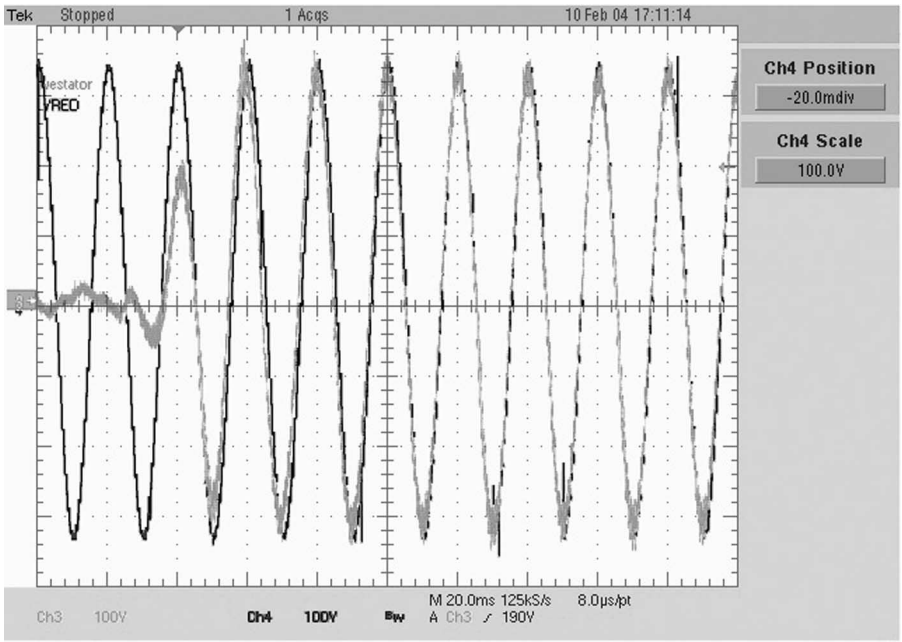

Fig. 5. Synchronization process at 1250 r/min.

although several specific functions have been developed in assembler.

Tuning equations (45) and (46) are applied to adjust the I-P controllers in charge of regulating $i_{rx'}$ and $i_{ry'}$ during synchronization. For this purpose, considering that rotor open-loop dynamics exhibit a $T_r = 119.6057$ ms time constant, a settling time of $t_{sd} = 100$ ms is accordingly demanded for closed-loop operation. Given that $\xi_d = 1$ is selected, a natural frequency of $\omega_{nd} = 58$ rad/s is required to satisfy the settling time specification. As a result, the parameters of the I-P controllers take the values $K_p = 2.2530$ V/A and $T_i = 31.9974$ ms.

Note that, once the DFIG stator is connected to the grid, its rotor open-loop dynamics turn out to be much faster, as they can be considered to be characterized by a $T_r' = 8.7713$ ms transient time constant. Consequently, a shorter closed-loop $t_{sd} = 25$ ms settling time is requested for current components i_{rx} and i_{ry}. Thus, according to [29], selection of $\xi_d = 1$ leads, for normal operation, to the parameter set $K_p = 0.5372$ V/A and $T_i = 6.5025$ ms.

Aiming to minimize unwanted rotor voltage "bumps" caused by transition between both sets of I-P controller parameters, the guidelines presented in point 4) of the previous section are applied. Besides, all I-P controllers are provided with antiwindup.

Both inputs to and outputs from the global control algorithm are easily identifiable from Figs. 1 and 4. Assuming balanced operation, it is sufficient to measure the stator and rotor currents, as well as the grid voltage of just two phases. Voltage sensors are also placed in two phases of the stator, whose measurements are required to execute initial rotor positioning. A 2048-pulse incremental encoder is used to derive both rotor mechanical position and speed. Processing of the encoder pulses is performed through the field-programmable gate array (FPGA) FLEX EPF 10K30AQC208-3 by Altera.

Starting from the rotor voltage $v_{r\alpha}$ and $v_{r\beta}$ output signals computed by the control program, an SVM algorithm—implemented in the same FPGA—generates the digital signals driving the insulated gate bipolar transistors (IGBTs) of the converter feeding the DFIG rotor. This SVM operates at a 2-kHz switching frequency.

B. Experimentation

A sample of the performance of the proposed synchronization algorithm at subsynchronous speeds is reflected in Fig. 5. During this test, the DFIG was actually forced by the dc drive to rotate at a 1250 r/min speed. For clarity, only phase "*A*" of both the grid voltage—in black—and the voltage induced at the open stator—in gray—are displayed. The time scale of the oscilloscope is set to 20 ms/division, while its vertical scale is set to 100 V/division.

The synchronization process is exactly launched at the 20th ms. It can be observed how the voltage induced at the phase "*A*" of the stator tracks the corresponding grid voltage and synchronizes to it as demanded, showing no overshoot and complying with the 100-ms closed-loop settling time specified when tuning the rotor $i_{rx'}$ and $i_{ry'}$ current I-P regulators.

Furthermore, an experiment demonstrating how the synchronization process runs satisfactorily even at supersynchronous speeds is illustrated in Fig. 6. In particular, the DFIG was driven at a 1650 r/min speed throughout this test. Even though the same vertical scale of 100 V/division is used, a 10 ms/division time scale is set in this case, aiming at achieving a more detailed portrait of the synchronization stage. Once again, the absence of overshoot and verification of the 100-ms closed-loop settling time specification can be corroborated.

Fig. 7 gives a good idea of the instantaneous stator current resulting when, after achieving synchronization, the DFIG stator is connected to the grid at zero power. In particular, the current in

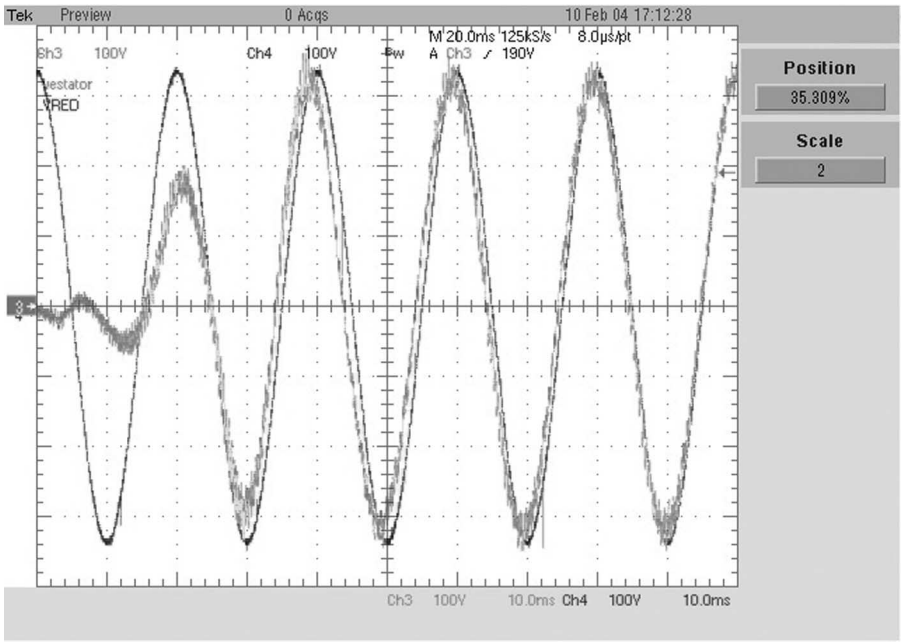

Fig. 6. Synchronization process at 1650 r/min.

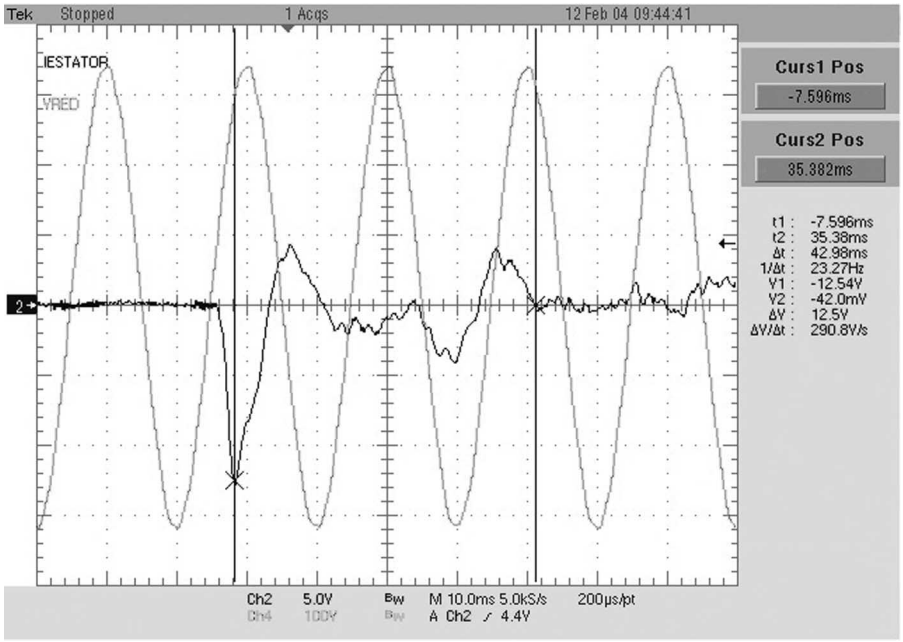

Fig. 7. Connection of the DFIG stator to the grid.

phase "*A*" of the stator—in black—is displayed together with the grid voltage of the same phase—in gray. Regarding current, the vertical scale of the oscilloscope is set to 0.5 A/division, while its time scale is again set to 10 ms/division. A current peak of about -1.25 A arises at the instant of connection. It should be noted that the latter figure only represents a 7.8% of the 16-A rated peak value of the stator current. In addition, it can also be observed how the stator current is regulated around zero after an initial transient lasting for about 45 ms, which corresponds to the settling time specified for the stator-side active and reactive power control loops in normal operation.

If three-phase voltage pulses of different amplitudes and frequencies are applied to the DFIG rotor in open loop, time responses of the rotor current and the voltage induced at the open stator like those in Fig. 8 can be observed. To avoid confusion, only the magnitudes corresponding to phase "*A*" are again provided. For current and voltage, 10 A/division and 100 V/division scales are, respectively, fixed, and the time scale is set to 100 ms/division. The signal with the lowest frequency—in black—is obviously the rotor current, which exhibits the slip frequency. Rotor current and stator voltage signals like those measured in such an experiment are more

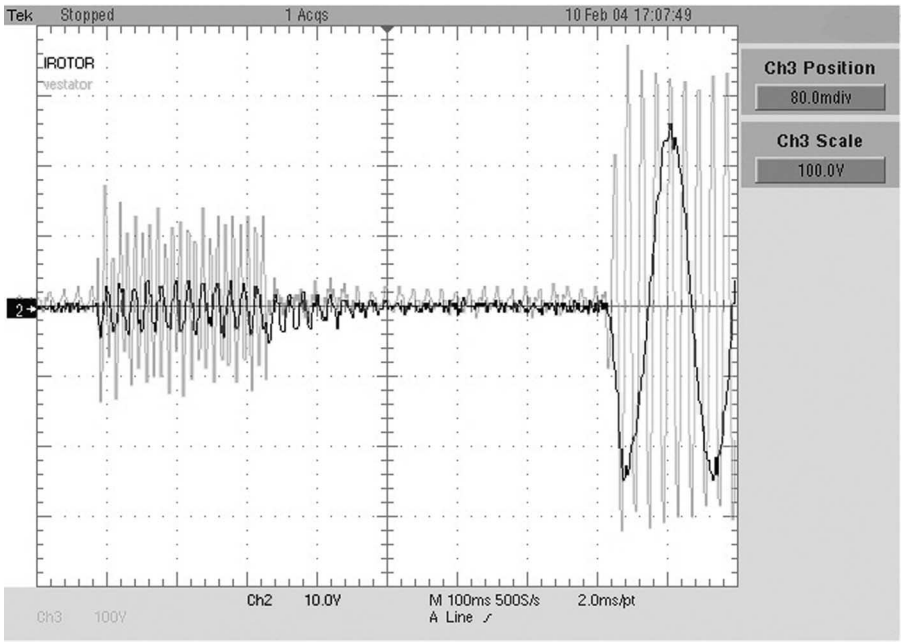

Fig. 8. Rotor current and induced stator voltage signals for initial rotor positioning.

than sufficient to carry out the proposed initial rotor positioning algorithm.

When selecting the amplitude and frequency of the open-loop three-phase voltage pulses to be applied to the rotor, it needs to be considered that the resulting voltage induced at the stator should be of reasonable amplitude and frequency. A steady-state analysis of expressions (28), (29), and (31) reveals that a rotor voltage of amplitude

$$|\vec{v}_r| = \sqrt{v_{rx'}^2 + v_{ry'}^2} = \frac{|\vec{v}_{\rm grid}|}{\omega_s L_m}\sqrt{R_r^2 + (\omega_{sl} L_r)^2} \qquad (54)$$

and frequency $\omega_{sl} = \omega_s - \omega_r$ must be applied to the rotor so as to induce a stator voltage of $|\vec{v}_{\rm grid}|$ amplitude and ω_s frequency. This is experimentally proved in the last 200 ms of the trial displayed in Fig. 8. In accordance, a voltage of predefined $|\vec{v}_s|_{\rm ref}$ amplitude and $\omega_{s\,\rm ref}$ frequency can be induced at the stator just by feeding the rotor with a voltage of

$$|\vec{v}_r| = \frac{|\vec{v}_s|_{\rm ref}}{\omega_{s\,\rm ref} L_m}\sqrt{R_r^2 + \left[(\omega_{s\,\rm ref} - \omega_r)\, L_r\right]^2} \qquad (55)$$

amplitude and $\omega_{s\,\rm ref} - \omega_r$ frequency.

An alternative solution consists in applying a closed-loop-controlled rotor voltage during initial rotor positioning. The same control scheme devoted to synchronization—see Fig. 4—can be used for this purpose. The only difference lies in the fact that θ_{ri} is obviously unknown prior to launching the initial rotor positioning process. This is not a problem, since it can actually be set to any value, for example, 0 rad. No matter the value assigned to θ_{ri}, the voltage induced at the stator will have the same amplitude and frequency of the grid voltage. It is also true that, depending on this value, a smaller or larger phase shift will arise between the grid and stator voltages. However, note that the latter is of no relevance at this stage, whose only objective is to induce a stator voltage of reasonable amplitude and frequency, which facilitates reliable estimation of initial rotor position.

The solution described before is adopted here, with θ_{ri} set to 0 rad. Note that, if a stator voltage of $|\vec{v}_s|_{\rm ref}$ amplitude was to be induced, it would be sufficient to replace the set point of $i_{rx'}$ in Fig. 4 with set point $i_{rx'\,\rm ref} = |\vec{v}_s|_{\rm ref} / (\omega_s L_m)$.

Of course, there is no way of knowing for sure if the value θ_{ri}, which is estimated during initial rotor positioning, is acceptable until the vector control algorithms for synchronization and normal operation are run. Note that, if the value derived for θ_{ri} was incorrect, a constant offset would arise between the actual rotor electrical position θ_r and that resulting from adding θ_{ri} to the signal provided by the encoder $\Delta\theta_r$.

As far as synchronization is concerned, θ_r is involved in the calculation of rotor current components $i_{rx'}$ and $i_{ry'}$, as well as in the demodulation of the three-phase voltage to be applied to the rotor—see Fig. 4. Consequently, a constant offset in the estimated rotor electrical position would lead to an induced stator voltage whose magnitude and frequency coincide with those of the grid voltage, but showing a phase shift with respect to the latter. Given that satisfactory synchronization is achieved in the tests reflected in Figs. 5 and 6, it follows that the value estimated for θ_{ri} at the end of the initial rotor positioning stage must, therefore, be acceptable.

With the aim of further supporting the effectiveness of the method proposed for initial rotor positioning, the results of an experiment carried out under normal operation are reflected in Fig. 9. The DFIG is required to generate 3 kW with no reactive power exchange between its stator and the grid. The waveforms corresponding to the "*A*" phase of the grid voltage—in gray—and the stator current—in black—are displayed on the upper part of the oscilloscope screen. Vertical scales of 200 V/division and 5 A/division are, respectively, set for voltage and current, and a 20 ms/division time scale is adopted in this case. In addition,

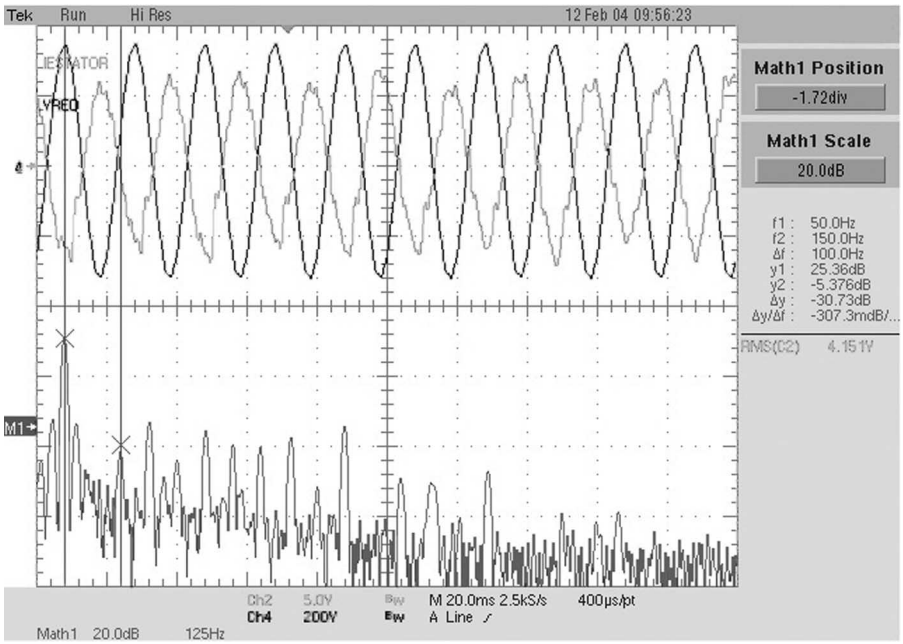

Fig. 9. Generation of a 3-kW active power with unity power factor.

the lower part of the screen is devoted to show the frequency spectrum of the resulting stator current waveform. Horizontal and vertical scales are set to 125 Hz and 20 dB, respectively. The cursor "M1" points to the gain level regarded as 0 dB.

A phase shift of 180^{o} between the grid voltage and the stator current waveforms is clearly observable, which corresponds to a DFIG generating power with unity power factor. Again, if rotor electrical position θ_r had been worked out based on an erroneous estimation of θ_{ri}, unexpected coupling between stator-side active and reactive power control loops would have arisen. In this particular test, the latter would have eventually resulted in an unwanted exchange of reactive power between the DFIG stator and the grid. Since this is obviously not the case, it must once more be concluded that the method suggested for initial rotor positioning leads to satisfactory performance.

VII. Conclusion

A systematic methodology for smooth connection of DFIGs to the grid has been presented. Experimental results support the appropriateness of the proposed overall method, which guarantees that, at the moment of connection, the current flowing between the DFIG stator and the grid turns out to be negligible. Although in variable-speed wind turbines the order of connection is typically generated at subsynchronous speeds, the suggested methodology is general, and could even be applied if DFIGs were to be connected to the grid at supersynchronous speeds.

A particular grid-voltage-oriented reference frame has been chosen to synthesize the vector control algorithm in charge of synchronizing the voltage induced at the DFIG open stator to that of the grid. Taking into account the dynamics exhibited by the DFIG rotor when its stator is disconnected from the grid, generic tuning equations have been derived for the I-P rotor current regulators present in the developed vector control scheme.

In addition to being suitable for the synchronization process itself, the specific reference frame considered at the synchronization stage facilitates a natural transition between the control configurations applied during synchronization and normal operation. In fact, once synchronization is achieved, the grid-voltage- and stator-flux-oriented reference frames coincide. Furthermore, the values of the rotor current components to be requested for zero-power connection are also coincident with the actual rotor current components resulting after achieving synchronization.

When the DFIG stator is open, its rotor dynamics exhibit a time constant of $T_r = L_r/R_r$, which turns into transient time constant $T'_r = L'_r/R_r$ when connecting the stator to the grid. In general, T_r turns out to be considerably larger than T'_r. As a consequence, when the DFIG stator remains open, the closed-loop response demandable to rotor current is not as fast as that achievable when it is connected to the grid. This leads to different values being assigned to the parameters of the rotor current I-P controllers, depending on whether the DFIG stator is connected to the grid or not. Simple rules ensuring "bumpless" transition between controllers at the instant of connection have been proposed. Application of these rules prevents the smoothness of the connection from becoming spoiled by the sudden change of controller parameters.

Even though wind-turbine-driven DFIGs are, in fact, asynchronous machines, they are compelled to operate as if they were synchronous. This implies that accurate knowledge of the initial rotor position is mandatory prior to launching any vector control algorithm based on the incremental encoder. A straightforward method has been suggested, which allows deriving the instantaneous rotor position when the DFIG stator is open, just before initiating the synchronization process. For the sake of

precision, this initial positioning task is carried out each time the control system of the DFIG generates a new order of connection. In contrast, initial rotor positioning is not required for "sensorless" schemes, since, in that case, the estimated electrical position of the rotor converges spontaneously to its actual value.

ACKNOWLEDGMENT

The authors would like to thank P. García de Madinabeitia, from JEMA, for all the help and advice kindly provided while developing the research work presented in this paper.

REFERENCES

[1] H. L. Nakra and B. Dubé, "Slip power recovery induction generators for large vertical axis wind turbines," *IEEE Trans. Energy Convers.*, vol. 3, no. 4, pp. 733–737, Dec. 1988.

[2] R. Peña, J. C. Clare, and G. M. Asher, "Doubly fed induction generator using back-to-back PWM converters and its application to variable-speed wind-energy generation," in *Proc. Inst. Electr. Eng. Electr. Power Appl.*, vol. 143, no. 3, pp. 231–241, May 1996.

[3] J. B. Ekanayake, L. Holdsworth, X. Wu, and N. Jenkins, "Dynamic modeling of doubly fed induction generator wind turbines," *IEEE Trans. Power Syst.*, vol. 18, no. 2, pp. 803–809, May 2003.

[4] W. E. Leithead and B. Connor, "Control of variable speed wind turbines: Design task," *Int. J. Control*, vol. 73, no. 13, pp. 1189–1212, Sep. 2000.

[5] G. Tapia, A. Tapia, and J. X. Ostolaza, "Proportional-integral regulator-based approach to wind farm reactive power management for secondary voltage control," *IEEE Trans. Energy Convers.*, vol. 22, no. 2, pp. 488–498, Jun. 2007.

[6] S. Peresada, A. Tilli, and A. Tonielli, "Indirect stator flux-oriented output feedback control of a doubly fed induction machine," *IEEE Trans. Control Syst. Technol.*, vol. 11, no. 6, pp. 875–888, Nov. 2003.

[7] S. Peresada, A. Tilli, and A. Tonielli, "Power control of a doubly fed induction machine via output feedback," *Control Eng. Practice*, vol. 12, no. 1, pp. 41–57, Jan. 2004.

[8] H. De Battista, P. F. Pauleston, R. J. Mantz, and C. F. Christiansen, "Sliding mode control of wind energy systems with DOIG—Power efficiency and torsional dynamics optimization," *IEEE Trans. Power Syst.*, vol. 15, no. 2, pp. 728–734, May 2000.

[9] H. De Battista, R. J. Mantz, and C. F. Christiansen, "Dynamical sliding mode power control of wind driven induction generators," *IEEE Trans. Energy Convers.*, vol. 15, no. 4, pp. 451–457, Dec. 2000.

[10] G. Tapia and A. Tapia, "Wind generation optimisation algorithm for a doubly fed induction generator," *Proc. Inst. Electr. Eng. Generation, Transmiss. Distrib.*, vol. 152, no. 2, pp. 253–263, Mar. 2005.

[11] H. Camblong, G. Tapia, and M. Rodríguez, "Robust digital control of a wind turbine for rated-speed and variable-power operation regime," *Inst. Electr. Eng. Control Theory Appl.*, vol. 153, no. 1, pp. 81–91, Jan. 2006.

[12] R. Cárdenas, R. Peña, J. Proboste, G. Asher, and J. Clare, "Rotor current based MRAS observer for doubly-fed induction machines," *Inst. Electr. Eng. Electron. Lett.*, vol. 40, no. 12, pp. 769–770, Jun. 2004.

[13] R. Peña, R. Cárdenas, J. Proboste, G. Asher, and J. Clare, "Sensorless control of doubly-fed induction generators using a rotor-current-based MRAS observer," *IEEE Trans. Ind. Electron.*, vol. 55, no. 1, pp. 330–339, Jan. 2008.

[14] R. Cárdenas, R. Peña, G. Asher, J. Clare, and J. Proboste, "MRAS observers for sensorless control of doubly-fed induction generators," *IEEE Trans. Power Electron.*, vol. 23, no. 3, pp. 1075–1084, May 2008.

[15] R. Cárdenas, R. Peña, J. Proboste, G. Asher, and J. Clare, "MRAS observer for sensorless control of standalone doubly fed induction generators," *IEEE Trans. Energy Convers.*, vol. 20, no. 4, pp. 710–718, Dec. 2005.

[16] R. Cárdenas, R. Peña, G. Asher, J. Clare, and J. Cartes, "MRAS observer for doubly fed induction machines," *IEEE Trans. Energy Convers.*, vol. 19, no. 2, pp. 467–468, Jun. 2004.

[17] F. Bonnet, P.-E. Vidal, and M. Pietrzak-David, "Dual direct torque control of doubly fed induction machine," *IEEE Trans. Ind. Electron.*, vol. 54, no. 5, pp. 2482–2490, Oct. 2007.

[18] S. Arnaltes and J. L. Rodríguez, "Grid synchronisation of doubly fed induction generators using direct torque control," in *Proc. IEEE 2002 28th Annu. Conf. Ind. Electron. Soc. (IECON 2002)*, Sevilla, Spain, Nov., pp. 3338–3343.

[19] X. Zhang, D. Xu, Y. Lang, and H. Ma, "Study on stagewise control of connecting DFIG to the grid," in *Proc. CES/IEEE 5th Int. Power Electron. Motion Control Conf. (IPEMC 2006)*, Shanghai, China, Aug., vol. 1, pp. 1–5.

[20] F. Blaabjerg, R. Teodorescu, M. Liserre, and A. V. Timbus, "Overview of control and grid synchronization for distributed power generation systems," *IEEE Trans. Ind. Electron.*, vol. 53, no. 5, pp. 1398–1409, Oct. 2006.

[21] A. G. Abo-Khalil, D.-C. Lee, and S.-H. Lee, "Grid connection of doubly-fed induction generators in wind energy conversion system," in *Proc. CES/IEEE 5th Int. Power Electron. Motion Control Conf. (IPEMC 2006)*, Shanghai, China, Aug., vol. 3, pp. 1–5.

[22] G. Iwanski and W. Koczara, "Synchronization and mains outage detection for controlled grid connection of the wind driven variable speed power generation system," in *Proc. Int. Conf. Clean Electr. Power (ICCEP 2007)*, Capri, Italy, May, pp. 585–590.

[23] G. Iwanski and W. Koczara, "PLL grid synchronization of the standalone DFIG based wind turbine or rotary UPS," in *Proc. Int. Conf. "Comput. Tool" (EUROCON 2007)*, Warsaw, Poland, Sep., pp. 2550–2555.

[24] P. Vas, *Sensorless Vector and Direct Torque Control*. New York: Oxford Univ. Press, 1998.

[25] P. Vas, *Vector Control of AC Machines*. New York: Oxford Univ. Press, 1990.

[26] H. W. van der Broeck, H.-C. Skudelny, and G. V. Stanke, "Analysis and realization of a pulsewidth modulator based on voltage space vectors," *IEEE Trans. Ind. Appl.*, vol. 24, no. 1, pp. 142–150, Jan. 1988.

[27] K. Zhou and D. Wang, "Relationship between space-vector modulation and three-phase carrier-based PWM: A comprehensive analysis," *IEEE Trans. Ind. Electron.*, vol. 49, no. 1, pp. 186–196, Feb. 2002.

[28] A. Tapia, G. Tapia, J. X. Ostolaza, and J. R. Sáenz, "Modeling and control of a wind turbine driven doubly fed induction generator," *IEEE Trans. Energy Convers.*, vol. 12, no. 2, pp. 194–204, Jun. 2003.

[29] G. Tapia, A. Tapia, and J. X. Ostolaza, "Two alternative modeling approaches for the evaluation of wind farm active and reactive power performances," *IEEE Trans. Energy Convers.*, vol. 21, no. 4, pp. 909–920, Dec. 2006.

[30] K. Ogata, *Modern Control Engineering*. Englewood Cliffs, NJ: Prentice-Hall, 2001.

[31] B. C. Kuo, *Digital Control Systems*. New York: Oxford Univ. Press, 1992.

[32] D. Ibrahim, *Microcontroller Based Applied Digital Control*. Chichester, U.K.: Wiley, 2006.

Gerardo Tapia was born in San Sebastián, Spain, on April 22, 1970. He received the Electr. Eng. degree from the University of Navarre, Donostia-San Sebastián, Spain, in 1995, the M.Sc. degree in digital systems engineering from Heriot-Watt University, Edinburgh, U.K., in 1996, and the Ph.D. degree from the University of the Basque Country, Donostia-San Sebastián, Spain, in 2001.

During 1997, he was an Assistant Researcher with Ikerlan Research Center, Spain. He is currently a Senior Lecturer in digital and advanced control theory, and control in embedded systems with the Department of Systems Engineering and Control, University of the Basque Country, Donostia-San Sebastián. His current research interests include wind power generation, control of rotary and linear electric drives based on sensorless vector and direct torque control schemes, and sliding-mode control.

Giovanna Santamaría was born in Barakaldo, Spain, on April 24, 1977. She received the Ind. Eng. degree from the University of the Basque Country, Bilbao, Spain, in 2002.

From January to September 2001, she was a scholarship student in the Department of Electrical Engineering, University of the Basque Country, Bilbao. In February 2003, she joined the R&D Department, Jesús María Aguirre, SA (JEMA), Lasarte-Oria, Spain. She is engaged in the development of control algorithms for solar converters, frequency converters, motor drives, and converters for railway applications. Her current research interests include wind power and photovoltaic generation, field-oriented control, and advanced control of renewable power generation.

Mikel Telleria was born in Tolosa, Spain, on March 19, 1976. He received the Mech. Eng. degree from the University of the Basque Country, Bilbao, Spain, in 2001, and the Electron. Autom. Eng. degree from Mondragon University, Mondragón, Spain, in 2002.

From 2002 to 2006, he was an R&D Project Manager at Jesús María Aguirre, SA (JEMA), Spain, where he was involved in the development of smart power converters. In 2006, he joined GAMESA, Sarriguren, Spain, where he is currently responsible for the 2-MW Wind Generator Product Improvement Team. His current research interests include wind power generation and multilevel power converters.

Mr. Telleria was awarded the Research Aptitude in Communications, Electronics and Control from the University of the Basque Country in 2005.

Ana Susperregui (M'06) was born in Irún, Spain, on October 13, 1974. She received the Ind. Electron. Tech. Eng. degree in 1998 and the Spec. Digit. Autom. Tech. degree in 1999 from the University of the Basque Country, Donostia-San Sebastián, Spain, where she is currently working toward the Ph.D. degree, and the Autom. Ind. Electron. Eng. degree from the University of the Basque Country, Bilbao, Spain, in 2003.

From January to September 1999, she was a scholarship student in the Department of Systems Engineering and Control, University of the Basque Country, Donostia-San Sebastián, where she was an Aggregate Professor until September 2000 and is currently an Associate Professor of classical control theory and industrial automation. In October 2002, she joined the VICOMTech Association, where she was an Assistant Researcher until September 2005. Her current research interests include standard and higher order sliding-mode control, advanced control of wind power generation systems, and remote monitoring.